Rheological characterization of nanostructured material based on Polystyrene-*b*-poly(ethylene-butylene)-*b*-polystyrene (SEBS) block copolymer: Effect of block copolymer composition and nanoparticle geometry

Noushin Hasanabadi [a], Hossein Nazockdast [a, *], Sandor Balog [b], Marco Lattuada [c, **]

[a] *Department of Polymer Engineering, Amirkabir University of Technology, Tehran, Iran*
[b] *Adolphe Merkle Institute, University of Fribourg, Chemin des Verdiers 4, CH-1700 Fribourg, Switzerland*
[c] *Department of Chemistry, University of Fribourg, Chemin du Musée 9, CH-1700 Fribourg, Switzerland*

Block copolymer (BCP) nanocomposite systems are of broad interest; however, reports on the role of nanoparticles on microphase separation behavior are rare. The goal of present study is to investigate the preparation of composite nanostructured materials containing Multi-Walled Carbon Nanotubes (MWCNTs) or graphene nanoplates. BCP nanocomposites based on the linear triblock copolymer, Polystyrene-*b*-poly(ethylene-butylene)-*b*-polystyrene (SEBS), with different morphological structure were prepared by melt mixing. The results of temperature sweep experiments showed an enhancing effect of both MWCNT and graphene nanosheets on increasing the microphase separation temperature as well as accelerating its kinetic, resulting from the confinement of BCP segments, with graphene nanosheets providing a more severely confined geometry for polystyrene segments in contrast to MWCNTs. Additionally, DMTA results indicated a promotion of the BCP microphase separation by incorporation of nanoparticles. Transient flow measurements followed by time sweep test suggested the existence of a special 3D network microstructure caused by nanoparticles/domain interactions.

1. Introduction

For many years, block copolymers (BCPs) have attracted considerable technological and scientific interests. This stems from their self-assembly into mesophases with one-, two- or three-dimensional periodic order. The ultimate morphology of block copolymers depends on the self-assembly phenomenon, which is governed by thermodynamic incompatibility, chain connectivity and relative length of blocks [1–8].

During the last decade, block copolymers have received special attention in the field of polymer nanocomposites due to their outstanding physical and mechanical properties. It has been shown that the presence of plate-like silicate layer in the BCP leads to materials with complex microstructure, whose detailed features depend on the degree of clay dispersion, microstructure of ordered domains and affinity between clay and individual blocks [9–14].

Carbon nanotubes (CNTs), because of their superb physical and mechanical characteristics have been used as one of the most useful building blocks candidates for producing new generation of composite materials for a variety of applications [15]. CNT can induce combinations of outstanding functional properties in the resulting nanocomposites [16,17]. However, the degree of success to achieve the prescribed targets greatly depends on the state of CNT dispersion, which is still a challenging issue for CNT filled polymer composites [18]. This is mainly due to the strong Van der Waals forces between nanotubes, which give rise to the formation of aggregates, thus leading to many defects in the final nanocomposite [19]. In this regard, BCPs may provide an ideal platform for the dispersion of CNTs, since one of the blocks might be designed to interact well with CNT's walls, while the other block can be used to induce the exfoliation of nanotubes by inducing repulsive interactions between polymer-wrapped nanotubes [20]. Peponi et al. [21] reported the use of dodecanethiol surfactant to sequester octadecylamine functionalized single-walled carbon nanotubes (ODA-SWCNTs) in the polystyrene phase of polystyrene-*b*-

* Corresponding author.
** Corresponding author.
  E-mail addresses: Nazdast@aut.ac.ir (H. Nazockdast), marco.lattuada@unifr.ch (M. Lattuada).

polyisoprene-*b*-polystyrene (SIS) block copolymer matrix, as demonstrated by the enhanced glass transition of PS phase and also morphological evolution by field-emission scanning electron microscopy (FE-SEM) [22]. Ilcikova et al. reported on the preparation of SIS BCP containing polystyrene-modified multiwalled carbon nanotubes. The presence of polystyrene chains on CNT surface improves the interaction at the filler-polymer interphase and facilitates their dispersion in SIS matrix confirmed by dynamic mechanical analysis [23].

Graphene, a monolayer of sp²-hybridized carbon atoms arranged in a two-dimensional honeycomb lattice is another reinforcing nanofiller that has attracted enormous interest during recent years due to marked enhancement in the polymer mechanical properties already at low filler fractions [18,24,25]. Although graphene has extensively been used as nanofiller to produce nanocomposites with significantly enhanced electrical and mechanical properties, the number of works using graphene in block copolymers is very low [26].

Polystyrene-*b*-poly(ethylene-butylene)-*b*-polystyrene (SEBS) are elastomeric BCPs with unique properties, targeting a variety of applications such as actuators, biomaterial, sensor, microcontact printing, etc. In SEBS BCP, the flexible rubber poly(ethylene-butylene) blocks are anchored on both sides by the glassy polystyrene blocks and various morphologies (spherical, cylindrical, lamellar) can be obtained by changing the molecular weight of the polystyrene domain.

The objective of the present study is to examine how the combination of the microstructure of SEBS block copolymers and the geometry of nanofiller (CNT and graphene) could influence the phase separation phenomena. In this paper, rheological measurements, due to their great sensitivity to microstructural changes, has been used as the main efficient tool in probing microstructure development of BCP hybrids [27]. The information extracted from rheological measurements has been complemented by means of both small angle x-ray scattering spectra and transmission electron microscopy images.

2. Experimental protocol

2.1. Materials

Three commercial Polystyrene-*b*-poly(ethylene-butylene)-*b*-polystyrene (SEBS), kindly supplied by Kraton Performance Polymers, Inc. were used in this work. SEBS G1657, G1652 and 1537 are linear triblock copolymers composed by 13 wt%, 30 wt% and 60 wt% polystyrene block respectively. It should be noted that SEBS 1537 has indeed 30 wt% PS in the end blocks and the remaining 30 wt% styrene is present in the almost random styrene/ethylene-butylene midblock. In order to improve phase separation, the amount of styrene in the SEBS 1537 just next to the PS end blocks is low.

Multi-Walled Carbon Nanotubes (MWCNTs) with the trade name of Nanocyl NC 700 (average diameter of 9.5 nm, average length of 1.5 μm and purity of 90%) and graphene nanosheets, N002-PDR, from Angstron Materials (thickness <1 nm, average diameter <10 μm, average aspect ratio of about 4000, surface area of 400–800 m² g⁻¹ and comprised of stacks of 1–3 monolayer graphene sheets) were used as the dispersed phase. SEM images of the pristine MWCNTs and graphene nanosheets are shown in Fig. 1a and b. SEM analysis was carried out on an AIS-2100 from Seron Co. (South Korea), operating at a voltage of 15 kV.

2.2. Nanocomposite samples preparation

All nanocomposite samples varying in MWCNT or graphene content were prepared using the melt-compounding method in a laboratory internal mixer (Brabender Plasticorder W50) at 220 °C with rotor speed of 80 rpm for 15 min.

2.3. Rheological measurements

Linear and non-linear viscoelastic measurements were performed using a rotational and oscillatory rheometer (Paar Physica UDS 200). All the measurements were conducted under nitrogen atmosphere using parallel plate geometry with a diameter of 25 mm and a constant 1 mm gap under controlled shear deformation oscillatory mode. The linear viscoelastic properties of samples were studied utilizing small amplitude oscillatory shear experiment over an angular frequency (ω) ranging from 0.05 to 1000 s⁻¹ and fixed strain (Y = 1%). Measurements made at lower strains were performed, but not used because of a too low signal-to-noise ratio. On the other hand, it was verified that all samples are in linear viscoelastic regime at a strain of 1%.

To study microphase separation of samples, temperature sweep experiments were performed at a strain of 1% and ω = 1 s⁻¹ and a cooling rate of 1 °C min⁻¹ under nitrogen purge to avoid oxidative degradation. Probing the transitional temperature by monitoring the low frequency storage modulus as a function of temperature during heating was not possible in our systems, due to the excessive normal force applied on the plates of the rheometer.

The structural evolution of SEBS G1652 nanocomposite samples were studied utilizing transient rheological experiments. Samples were initially subjected to shear flow with a constant shear rate 1 s⁻¹ for 500 s. Afterwards, in order to quantify the extent of block copolymer nanocomposite restructuring, a time sweep experiment was performed immediately after cessation of flow and storage and loss modulus was measured against time in an angular frequency of 1 s⁻¹.

Dynamic mechanical analysis (DMA) was performed by using a Diamond DMA Perkin Elmer analyzed in tensile mode at a frequency of 1 Hz, temperature range from −80 to 140 °C and heating rate of 5 °C min⁻¹ under nitrogen atmosphere using samples of (20 × 11 × 1 mm) cut from compression molded sheets.

2.4. SAXS measurements

The morphology of block copolymers and their nanocomposites samples were evaluated by small-angle X-ray scattering (SAXS). The SAXS spectra were recorded using a NanoMax-IQ camera (Rigaku Innovative Technologies, Auburn Hills, MI USA). The samples were kept under vacuum at room temperature during the measurements. The scattering spectra are presented as a function of momentum transfer, defined by q = $4\pi\lambda^{-1}$ sin(θ/2) (where θ is the scattering angle and λ = 0.1524 nm is the photon wavelength).

2.5. TEM images

Transmission electron microcopy (TEM) images of the neat BCPs and of the nanocomposite have been acquired by means of a JEOL JEM 2100 operating at a voltage of 200 kV. The preparation of the samples has been carried out by sectioning the samples using an Ultracryomicrotome Leica EM UC7.

3. Results and discussions

3.1. TEM analysis

The objective of this work is the thorough characterization of possible phase changes in microstructure and phase changes in BCP

upon the addition of unmodified CNTs and graphene nanosheets. Since all the nanocomposite samples have been prepared by melt compounding, we first performed a characterization by means of TEM. Due to the elastomeric nature of the block copolymers, TEM sample preparation required sectioning the nanocomposites using an ultracryomicrotome. TEM images of selected samples are presented in Fig. 1. These images (c-e) show that the block copolymers structure is barely visible without the use of staining, even though some structural feature can be discerned. More interesting are the images (f-h) of the nanocomposites, clearly showing a good dispersion of both CNTs (f-g) and graphene nanosheets (h). At the same time, no preferential positioning of CNTs and graphene nanosheets in some block is visible, thus suggesting the tendency of all nanofillers to position themselves across the various BCP domains, and to form interconnected networks (visible in Fig. 1f and g). These findings confirm that the melt compounding procedure used to prepare the nanocomposites is effective in dispersing CNTs and graphene nanosheets into the BCP matrices.

3.2. Morphological structure of BCPs by means of SAXS

Since TEM cannot be used to clarify the morphology of the BCPs, and the effect of nanofillers, SAXS has been used for this purpose. Fig. 2 presents 1D SAXS plots for neat BCPs and their nanocomposite samples containing 0.5 wt% CNT or graphene nanoparticles. SAXS pattern is extensively used to identify the structural morphology in BCP samples from the sequence of Bragg reflection observed [37].

As it is observed in SEBS 1657 and SEBS 1652 SAXS patterns, Bragg peak maxima space at angles for which the ratios q_n/q_1 are equal to $1, \sqrt{3}, \sqrt{7}$, indicating that both BCPs consist of cylindrical domains spatially arranged in a 2-D hexagonal lattice. It is worthnoting that by room temperature cooling used here (the prepared samples were subjected to room temperature immediately after processing at the temperature of 220 °C), SEBS 1657 could not order PS sphere domains in to the BCC lattice as the time required for spherical ordering was not sufficiently long before the vitrification PS domains [38].
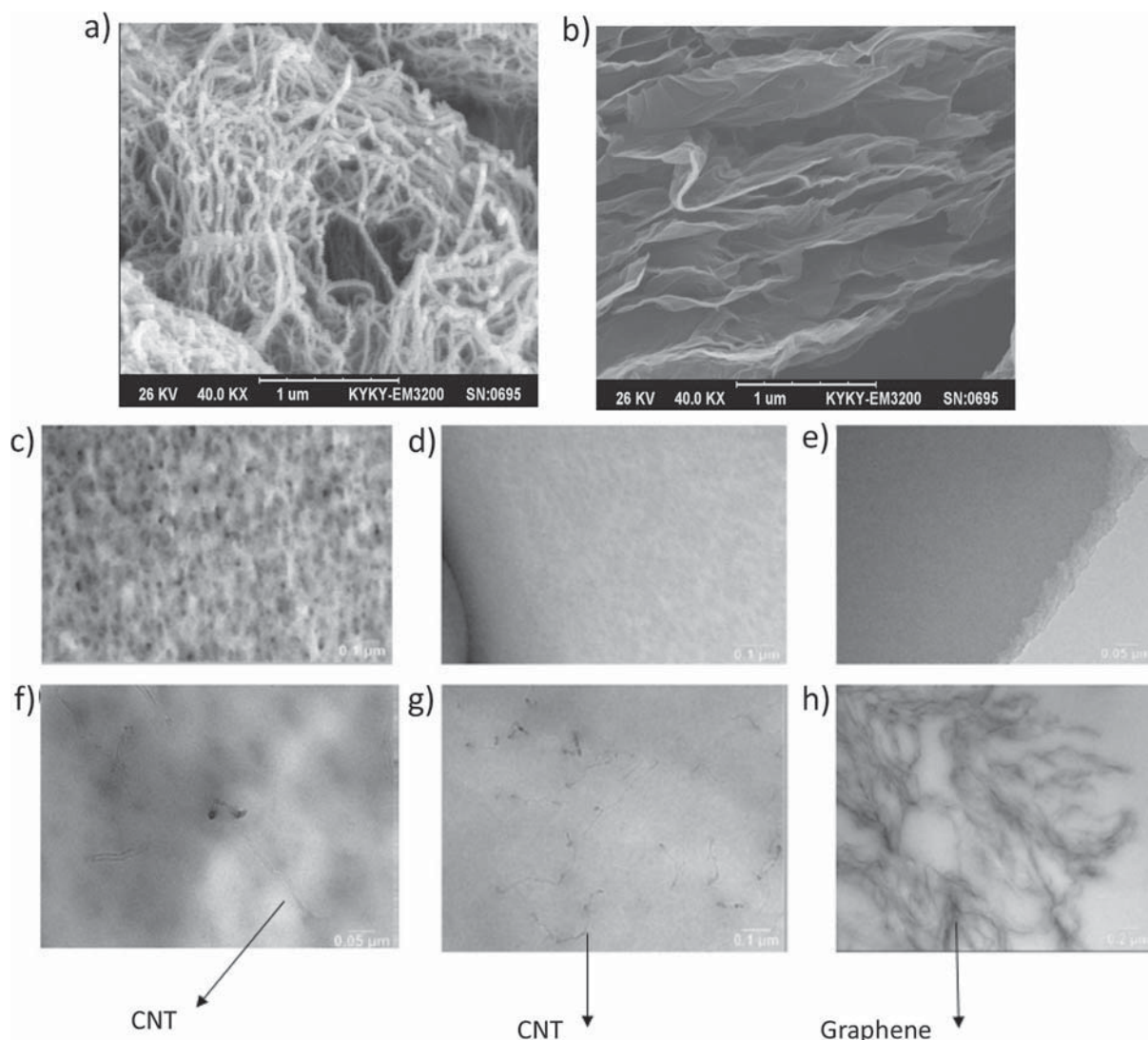
Fig. 1. SEM images of: (a) MWCNTs, (b) graphene nanosheets, TEM images of BCPs and their composites: (c) neat SEBS 1537, (d) SEBS 1652, (e) SEBS 1657, (f) SEBS 1537 0.5 w% CNT, (g) SEBS 1652 0.5 w% CNT, (h) SEBS 1657 0.5 w% graphene nanosheets.
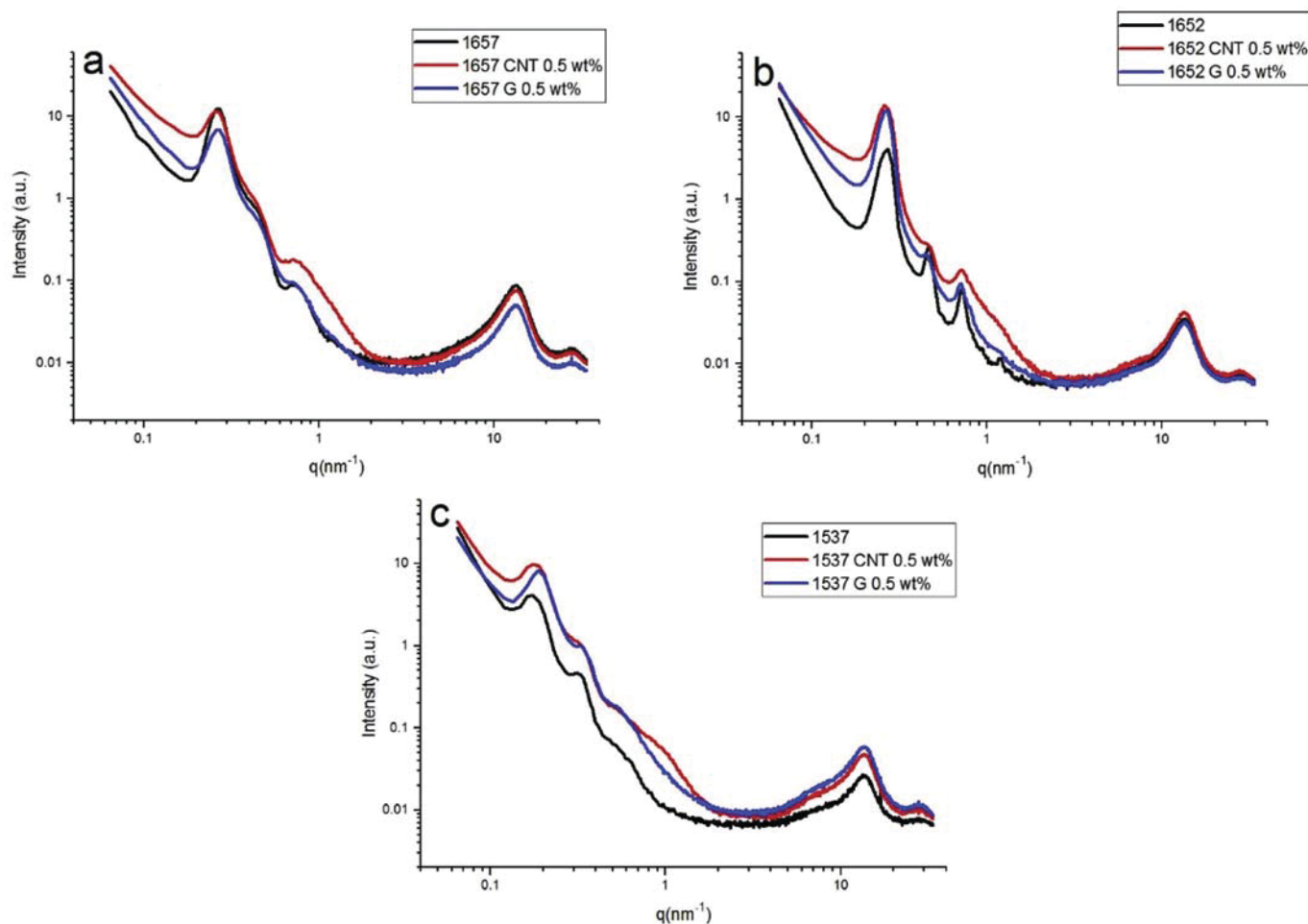
Fig. 2. 1D SAXS plots for (a) SEBS 1657, (b) SEBS 1652, and (c) SEBS 1537 neat BCPs and their nanocomposite samples containing 0.5 wt% nanofillers.

The SAXS pattern of SEBS 1537 reveals a set of Bragg peaks associated with lamellar morphology.

From angular averaged SAXS profiles, it can be noticed that no changes were observed in the feature of the SAXS patterns upon incorporation of CNT or graphene nanoparticles, thus suggesting the BCPs retain their original structure and addition of nanoparticles could not disrupt the BCP ordering.

3.3. Melt state rheological behavior

In order to gain better characterization of the polymer structure and also of the state of nanoparticles dispersion, linear viscoelastic behavior of materials has been investigated using melt rheology.

Fig. 3 shows the results of storage modulus, G′, as function of frequency (ω) for the neat SEBS (G1657, G1652 and 1537) samples measured at 220 °C. It can be seen that the SEBS G1657 shows a terminal behavior in the storage modulus vs. frequency at low frequencies ($G' \sim \omega^2$) which is the characteristic of block copolymers in their disordered state while SEBS G1652 and SEBS 1537 show a non-terminal behavior. Similar results have been reported in the literature, where this was attributed to the 3-D network structure formed by the domain interconnectivity, which is not completely destroyed even at 220 °C [11]. It can be observed that SEBS G1652 is in the cylindrical ordered state, recognizable by the slope of 0.21, which is the characteristic of block copolymer with cylindrical microstructure. The storage modulus curve of SEBS 1537 is typical of an ordered lamella structure having a non-terminal behavior scaling as $G' \sim \omega^{0.5}$ [11].

It has been well recognized that the addition of nanoparticles can have an appreciable effect on the morphological development of multiphase polymeric material [27]. The results of similar experiment performed on SEBS G1657, SEBS G1652 and SEBS 1537 nanocomposites containing different MWCNT loadings are shown in Fig. 4. It can be seen that while the 0.05 wt% MWCNT containing SEBS G1657 sample exhibit a rheological behavior similar to that of neat BCP SEBS G1657 matrix, the sample with 0.5 wt% MWCNT concentration shows a pronounced low frequency nonterminal storage modulus behavior whose extent is greatly enhanced in the case of 1 wt% MWCNT filled SEBS G1657 nanocomposite sample. Such a liquid-solid like transition is the indication of a strong three-dimensional network structure formed between MWCNT-MWCNT and/or MWCNT-matrix, which hinders the complete relaxation of the matrix chains.

As can be observed, in SEBS G1652 and SEBS 1537 nanocomposite samples, the low frequency non-terminal behavior increases as the content of MWCNT increases. By comparing the results obtained for SEBS G1652 and SEBS 1537 with those discussed for SEBS G1657, one may clearly notice that the effectiveness of addition of MWCNT on enhancing low frequency storage modulus decreases with increasing the ordering of block copolymers. These results can be explained in terms of the ability of BCP chains to disperse MWCNT. It is well-known that the state of
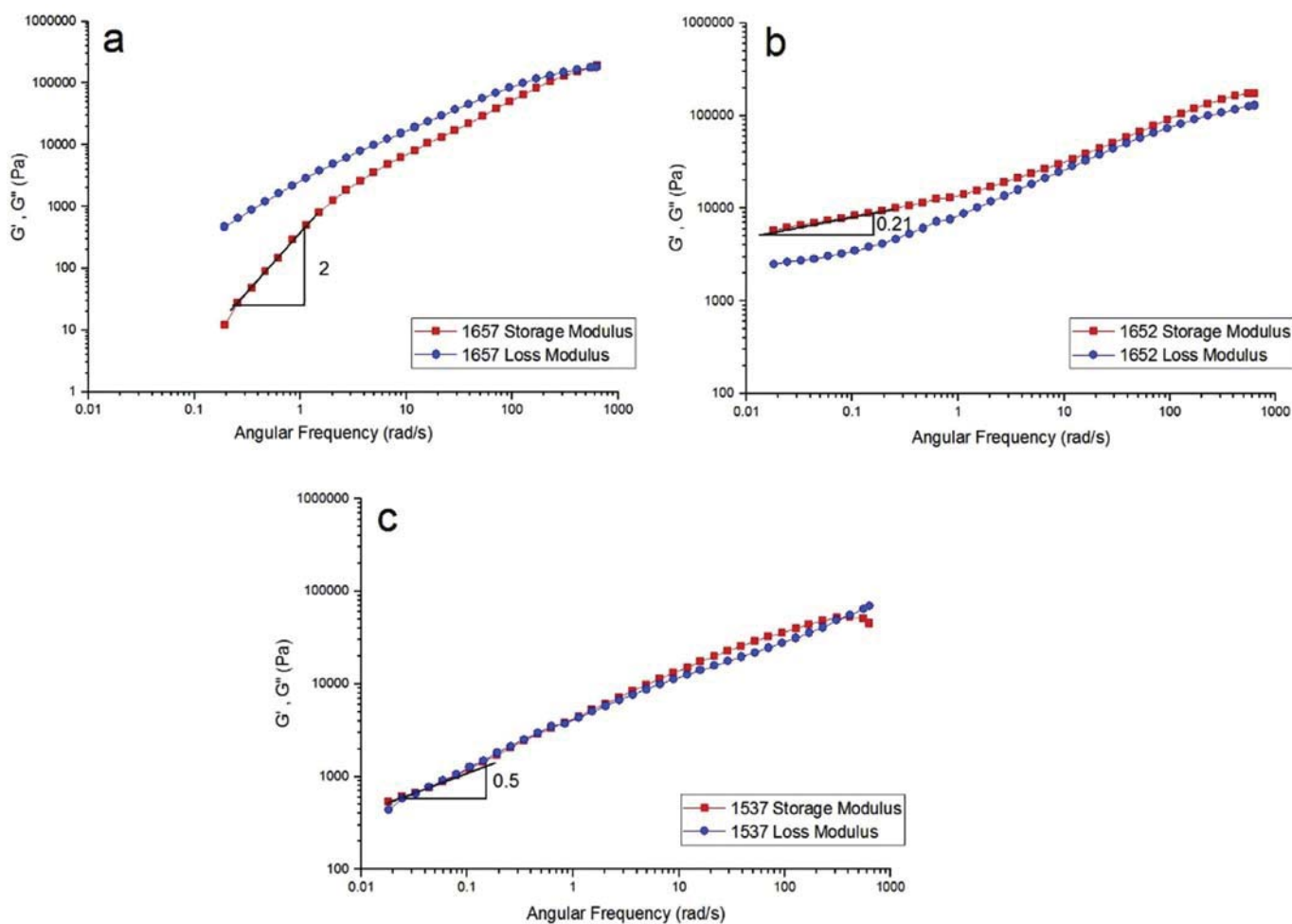
Fig. 3. Storage and Loss modulus as a functional frequency for neat block copolymers (a) SEBS 1657, (b) SEBS 1652, and (c) SEBS 1537, All measurements were carried out at 220 °C.

MWCNT dispersion is highly dependent on the ability of matrix chain molecules to diffuse in to CNT aggregates and force the CNTs to be uniformly dispersed. Thus, both the thermodynamic affinity between CNT and matrix and the matrix viscosity can play an important role in determining the degree of CNT dispersion.

Considering the viscoelastic results of the three BCPs discussed in Fig. 3, it appears that chain mobility of block copolymers decreases with microstructural formation. Therefore, the degree of MWCNT dispersion and hence, the extent of 3D network is expected to be reduced by increasing the microstructure ordering of BCP.

Linear viscoelastic results obtained for SEBS G1657, SEBS G1652 and SEBS 1537 samples containing graphene are shown in Fig. 5. As can be seen, SEBS G1657 nanocomposites containing graphene in contrary to MWCNT filled ones, show similar terminal rheological behavior to that neat BCP matrix. But in SEBS G1652 and SEBS 1537, the presence of nanosheets increases the storage modulus, especially in the low frequency region whose extent increases with the increase of graphene concentration. It is important to note that the effective dispersion of graphene nanosheets depends not only on the diffusion of polymer matrix between nanosheets, but also on the extent of convective forces applied to the system during melt mixing.

The absence of linear frequency elastic response in graphene filled SEBS G1657 indicates that the mentioned block copolymer chain molecules are not capable to intercalate graphene plates to form a 3D network structure. This is probably because the matrix viscosity and therefore, the shear stress involved during melt mixing are not high enough for intercalation. This is well evidenced by the results observed for SEBS G1652 and SEBS 1537 block copolymer nanocomposites (Fig. 5b and c) which show a pronounced non-terminal behavior as a results of high matrix viscosity and hence greater extent of intercalation compared to that of SEBS G1657.

It has been demonstrated that rheology can be employed to probe the microstructural evolution of partially miscible blends and block copolymers. There are several indicators of the transformations occurring at the microscale. The order-disorder temperature is one such indicator. It refers to the full transition between an ordered and a disordered state. For some block copolymers, however, a full disordered state cannot be reached even at high temperatures, before the block copolymer decomposes. Therefore, a different indicator is sometimes used: the microphase separation temperature, which is indicative of a transition between a fully ordered and a partial disordered state. The microphase separation temperature could be determined by monitoring the evolution of storage modulus as a function of temperature. Evidently, storage modulus linearly increases with decreasing the temperature due to the lower chain mobility (Brownian motion of the chains). As the temperature is decreased further and in the vicinity of phase separation temperature, a distinct change in slope is observed and storage modulus increases rapidly as a function of
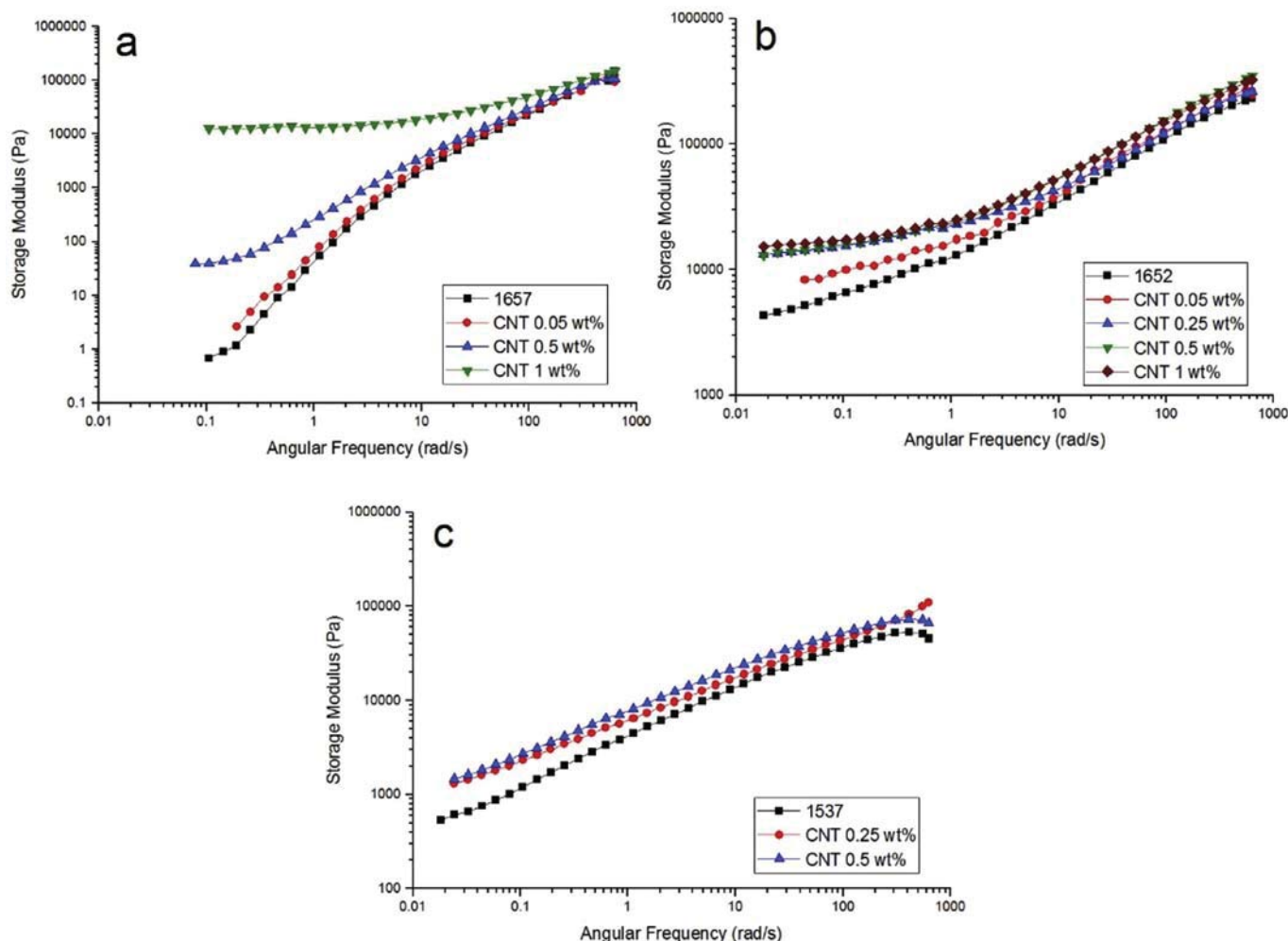
5

Fig. 4. Storage modulus as a functional frequency for (a) SEBS 1657, (b) SEBS 1652, and (c) SEBS 1537 nanocomposites containing MWCNT, All measurements were carried out at 220 °C.

temperature [28,29].

The results of temperature sweep experiments performed on block copolymers (SEBS 1657, SEBS 1652 and SEBS 1537) are shown in Fig. 6. As can be observed the lamellar block copolymer shows a sharp increase in storage modulus at temperature about 136 °C while the other two block copolymers show a smooth increase in storage modulus as they reach to their phase separation temperature. The figure also illustrates that SEBS 1537, 1652 and 1657 show microphase separation at 136 °C, 130 °C and 122 °C respectively. The temperature as well as kinetic of microphase separation is enhanced with increasing polystyrene content.

From the thermodynamic point of view, block copolymers with higher PS content are expected to exhibit higher microphase separation temperature with enhanced kinetic of microphase separation due to the enhanced segmental incompatibility, which is in favor of microphase separation process.

It should also be noted that the block copolymer with lamellar morphology tends to the same storage modulus values of block copolymer with cylindrical morphology. This can be attributed to strong three-dimensional network structure formed for cylindrical block copolymer compared to lamella block copolymer.

Fig. 7(a,b) compares the effect of addition of CNT and graphene on the microphase separation temperature of the sample SEBS G1657 measured by temperature sweep test. It could be observed that for both CNT and graphene filled samples, the addition of

nanofillers promotes microphase separation, and also that the presence of graphene has a greater influence on increasing the kinetics and the temperature of microphase separation temperature compared to that of CNT, even though the degree of dispersion of CNT is better than that of graphene. This can be explained in terms of greater extent of PS segments confinement in graphene interlayer space, which provides higher potential for PS domain formation in graphene filled sample compared to CNT. Such a confinement of PS segments leads to stretching of polymer chains and reducing the number of chain conformations. Hence, the enthalpic interactions begin to dominate and a microphase separated structure is formed. A similar behavior has also been observed on the crystalline behavior of nanocomposite samples containing CNT and graphene nanoplates [30,31].

The results of similar experiments obtained for cylindrical BCP nanocomposites are shown in Fig. 7c,d. It can be seen that both CNT and graphene have greater effect on enhancing the kinetic and temperature of microphase separation of BCP with cylindrical morphology as compared to BCP with spherical morphology. It can also be seen that graphene has greater enhancing efficiency on microphase separation temperature.

Due to higher concentration of PS segment in BCP with cylindrical microstructure, nanofillers can play more significant role in increasing the segmental incompatibility which leads to faster kinetic and higher microphase separation temperature. The greater
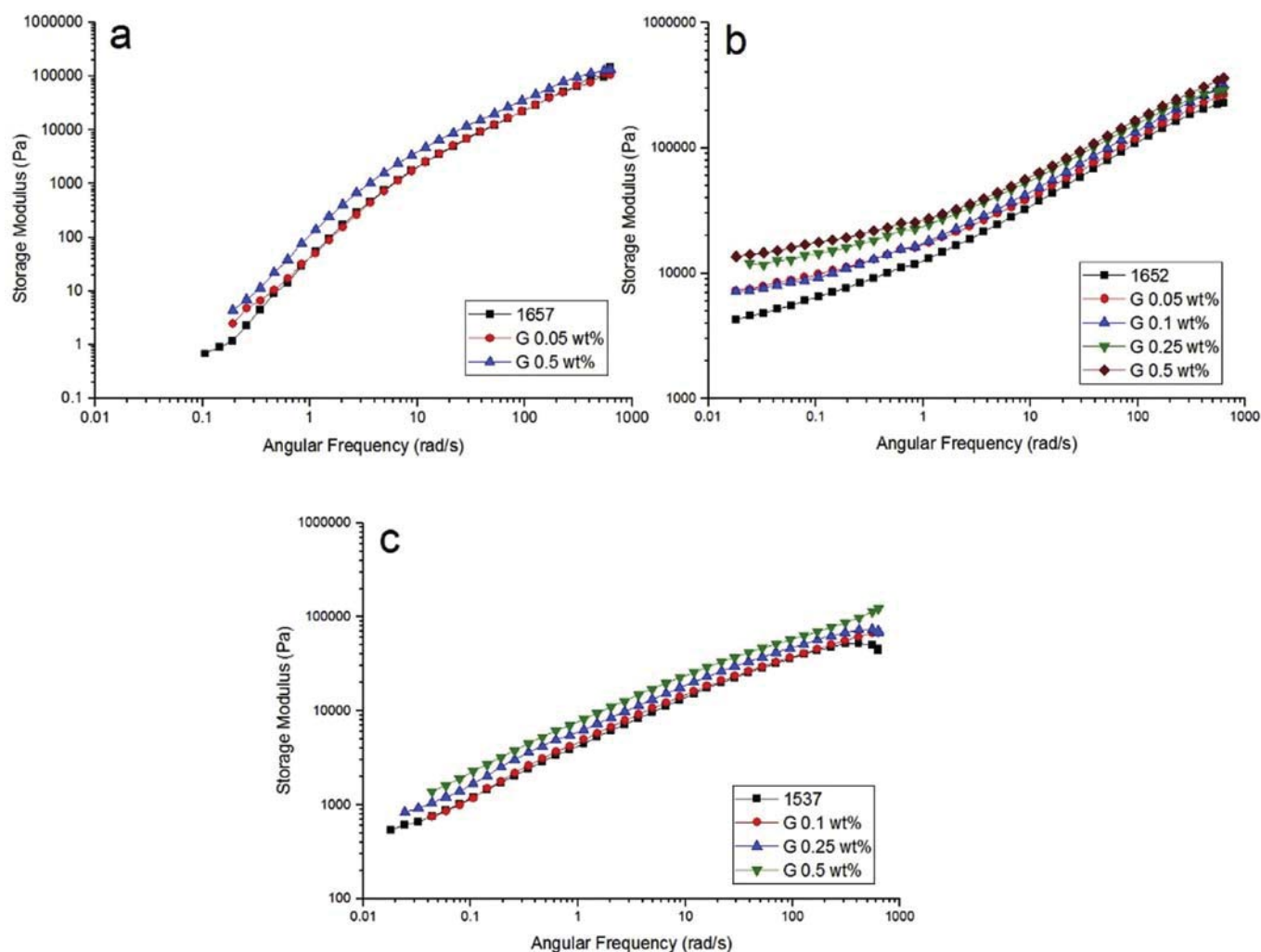
Fig. 5. Storage modulus as a functional frequency for (a) SEBS 1657, (b) SEBS 1652, and (c) SEBS 1537 nanocomposites containing graphene. All measurements were carried out at 220 °C.
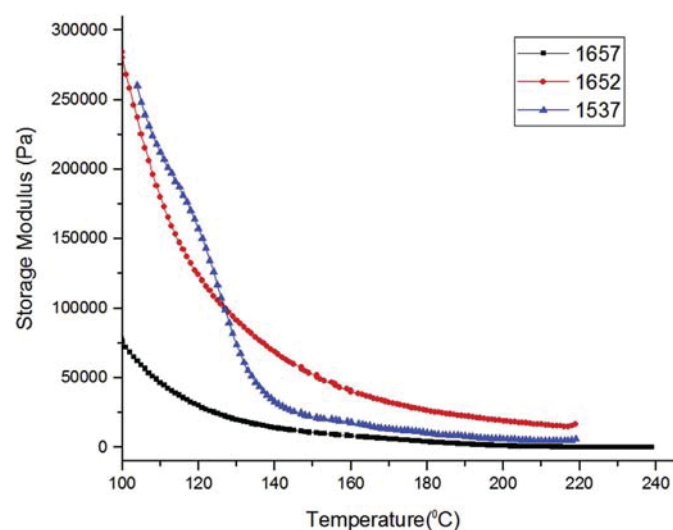

Fig. 6. Storage modulus versus temperature for neat block copolymers (SEBS 1657, SEBS 1652 and SEBS 1537).

effect of graphene on microphase separation compared to CNT observed for this sample can be attributed to higher extent of chain confinement between graphene nanoplates.

The results of temperature sweep experiments performed on SEBS 1537 BCP nanocomposite samples are displayed in Fig. 7e,f. It could be noted that, in contrast to the other two discussed BCP samples, the presence of nanofillers doesn't have appreciable influence on the microphase separation temperature of SEBS 1537 BCP. Table 1 list the microphase separation temperatures of all the samples analyzed in this work.

As discussed before, preferential interaction of nanofillers with PS segments would increase the segmental incompatibility which is in the favor of microphase separation. However, due to this kind of interaction, the motion of PS segments is dramatically restrained and chains lose their ability to form microdomain structures. Thus, according to the two opposing effects, the microphase separation ability of BCP remains unchanged.

3.4. Transient flow measurement

The BCPs nanocomposite materials containing anisotropic nanoparticles could undergo dramatic changes in their structure in response to external flow field. In addition to aligning the BCP
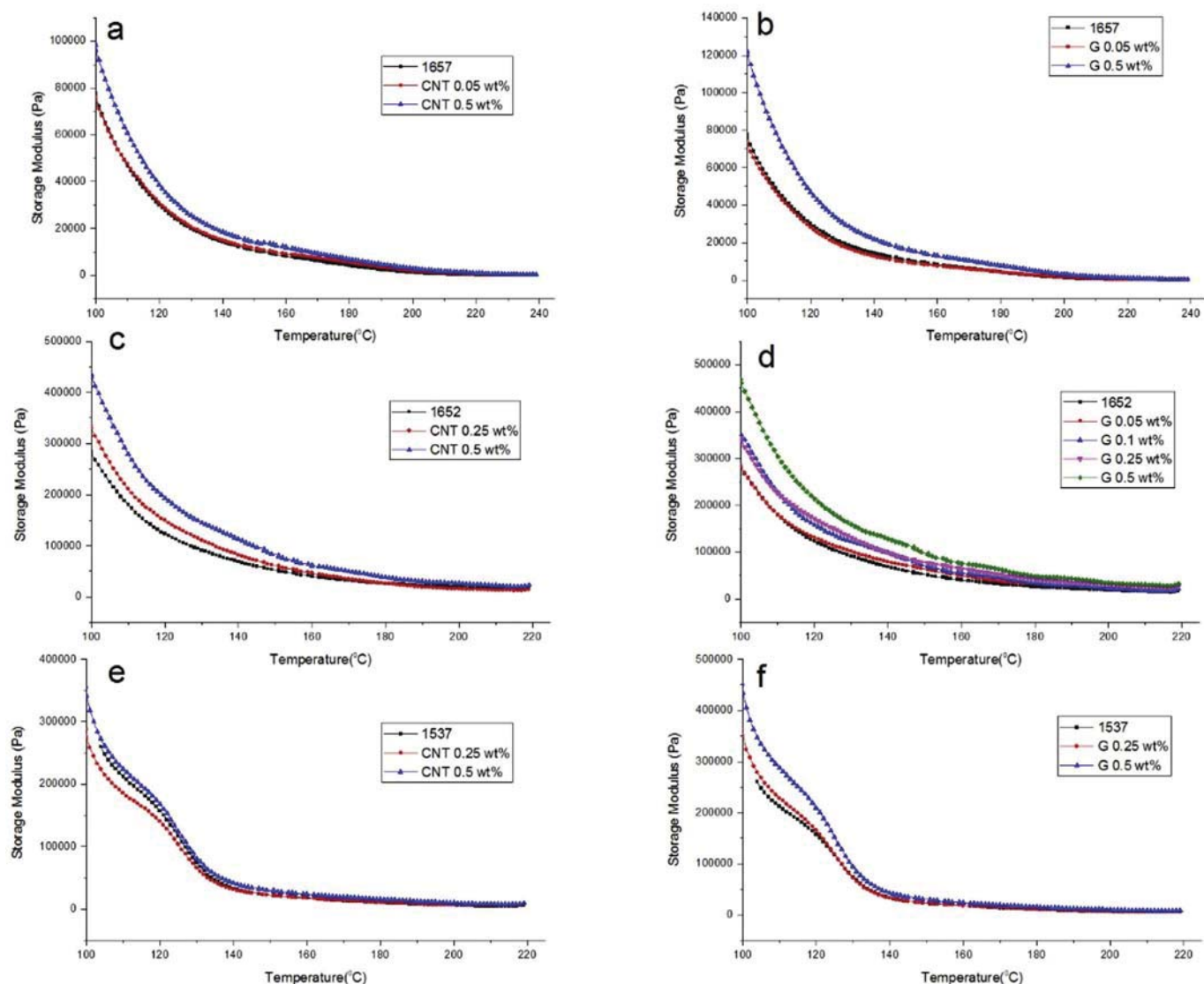
7

Fig. 7. Storage modulus versus temperature for SEBS G1657 nanocomposite samples containing a) MWCNT, b) graphene, SEBS G1652 nanocomposite samples containing c) MWCNT, d) graphene, SEBS 1537 nanocomposite samples containing e) MWCNT and d) graphene.

Table 1
Microphase separation temperature of nanocomposite samples.

Block Copolymer Grade	Microphase Separation Temperature							
	Neat BCP	BCP containing CNT			BCP containing Graphene nanosheets			
		0.05 wt%	0.25 wt%	0.5 wt%	0.05 wt%	0.1 wt%	0.25 wt%	0.5 wt%
SEBS G1657	122 °C	122.21 °C	–	127 °C	122.9 °C	–	–	126.75 °C
SEBS G1652	130 °C	–	133.7 °C	138.05 °C	135.53 °C	137.08 °C	140.06 °C	144.31 °C
SEBS 1537	136 °C	–	136 °C	137.86 °C	–	–	136 °C	137.18 °C

domains, the applied shear deformation can also induce the orientation of incorporated anisotropic nanoparticles.

The flow induced orientation of nanofillers and PS domains are two interrelated and yet complicated processes that can play a significant role on determining the kinetic and the extent of structural recovery of filled samples. In order to explore some understanding about this effect, the transient test comprising start up flow test followed by immediate time sweep test after cessation of flow as described in the experimental section [32–34]. These

rheological measurements provide precious information on the state of structural recovery during rest.

Fig. 8a shows the results of shear stress versus time measured at constant shear rate 1 s^{-1} for neat 1652 BCP and CNT containing nanocomposites. As can be seen, the neat BCP exhibits pronounced stress overshoot followed by a quick reduction to steady state shear stress. This behavior implies a three-dimensional type microstructure due to PS domains interconnectivity, which could thermodynamically persist up to 220 °C although with weaker
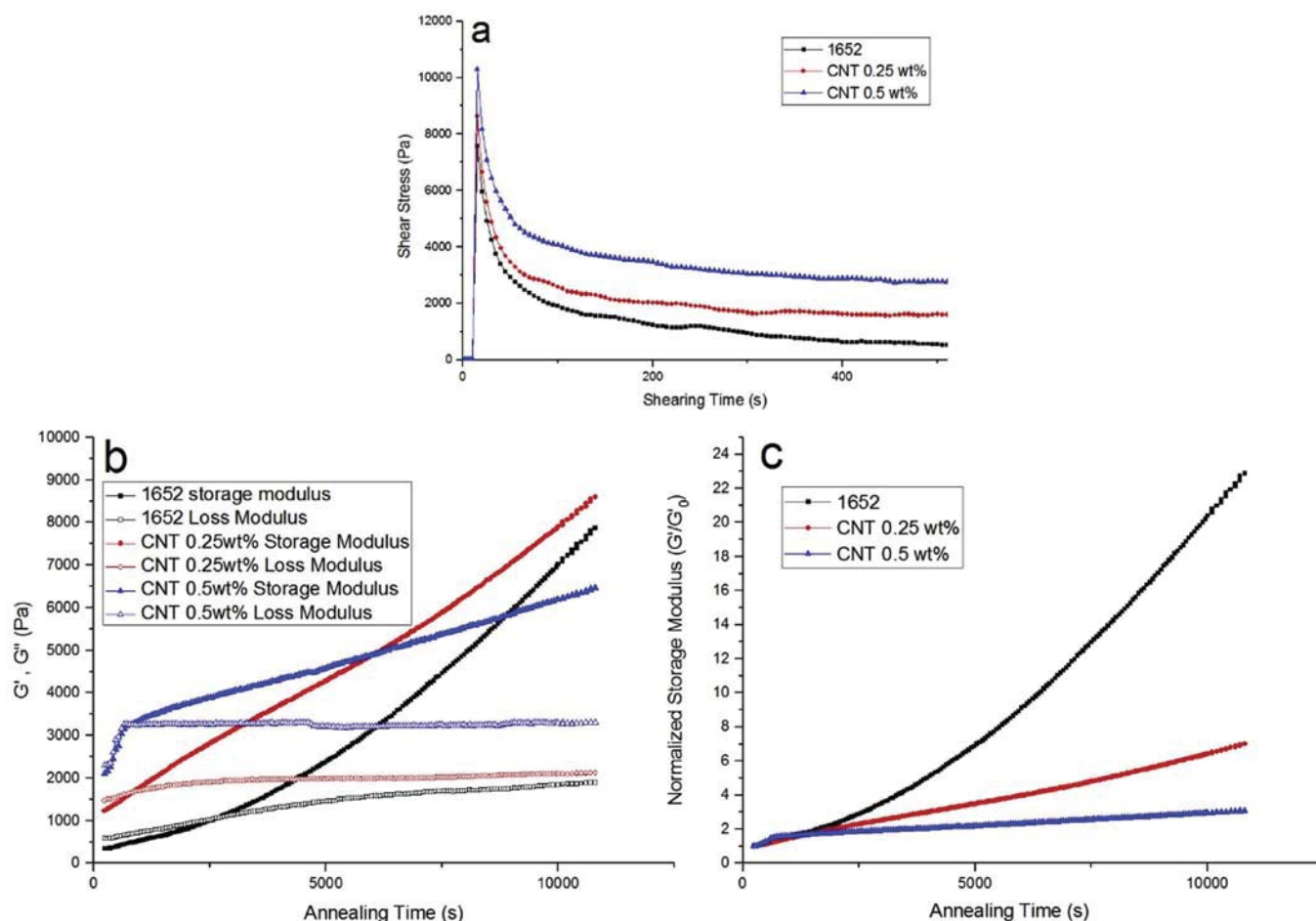
Fig. 8. a) Stress as a function of time, b) Storage and Loss modulus recovery, c) Normalized Storage Modulus after cessation of flow with shear rate of 1 s^{-1} for SEBS 1652 nanocomposite samples containing MWCNT at T = 220 °C.

strength. The CNT filled samples exhibit stronger stress overshoot and higher steady state stress, whose extent enhances with increasing CNT content.

The fact that CNT induce enhancing effects on stress overshooting can be attributed to strengthening of a special 3D network microstructure which could be generated either by CNT network structure or a stronger 3D network of block copolymer domains caused by nanofillers/domain interaction. The block copolymer segments confined between CNTs can form domains with stronger interfacial interaction with CNTs.

The higher steady state stress observed for CNT filled sample indicates that 3D network has not fully destroyed under the applied shear rate. This indicates an enhanced 3D structure of nanofilled samples as compared to unfilled sample due to stronger connection between domains in vicinity of CNTs, which support the above described mechanism.

In order to provide more insight into understanding the structural evolution of BCP nanocomposites, the time sweep experiments were performed on the samples after cessation of flow. Fig. 8b,c shows the recovery of storage modulus versus annealing time for the neat SEBS 1652 BCP and its nanocomposites containing CNT. It can be noticed that neat BCP exhibits a slow recovery rate at the beginning followed with a faster rate at longer annealing time.

AS can be seen in Fig. 8, the results also show that an addition of CNT to BCP leads to higher initial storage modulus compared to neat BCP and slower kinetic of restructuring, whose extent enhances with increasing CNT content.

In the case of neat BCP, randomization of domains takes place at short initial time by Brownian motion mechanism. After reorientation of nanodomains, the 3D network structure between reoriented domains would be formed, leading to a faster growth of the storage modulus.

The higher initial value of the storage modulus of nanocomposite samples is due to the incomplete structural breakdown during flow, according to a strong 3D network formed by CNT and block copolymer domains. Slower development of structures in nanocomposite samples indicates that the average relaxation time required increases by the presence of CNT, hence Brownian forces could not be the only involved mechanism. On the other hand, strong interfacial interaction between CNTs and the neighboring BCP domains play a significant role in structural reconstruction under quiescent condition. This phenomenon would explain the slowing effect of CNT on the kinetics of the structural evolution, whose extent becomes more obvious by increasing the CNT content. This is due to the increasing number of confining PS domains, which play a significant role in strengthening of CNT/BCP structure. It could also be observed that the nanocomposite sample containing 0.5 wt CNT exhibits a fast recovery of storage modulus at the initial stage. This suggests that there are some non-interacting CNT particles, restricted by BCP domains.

The results of similar experiments obtained for cylindrical BCP containing graphene nanosheets are shown in Fig. 9. The similar
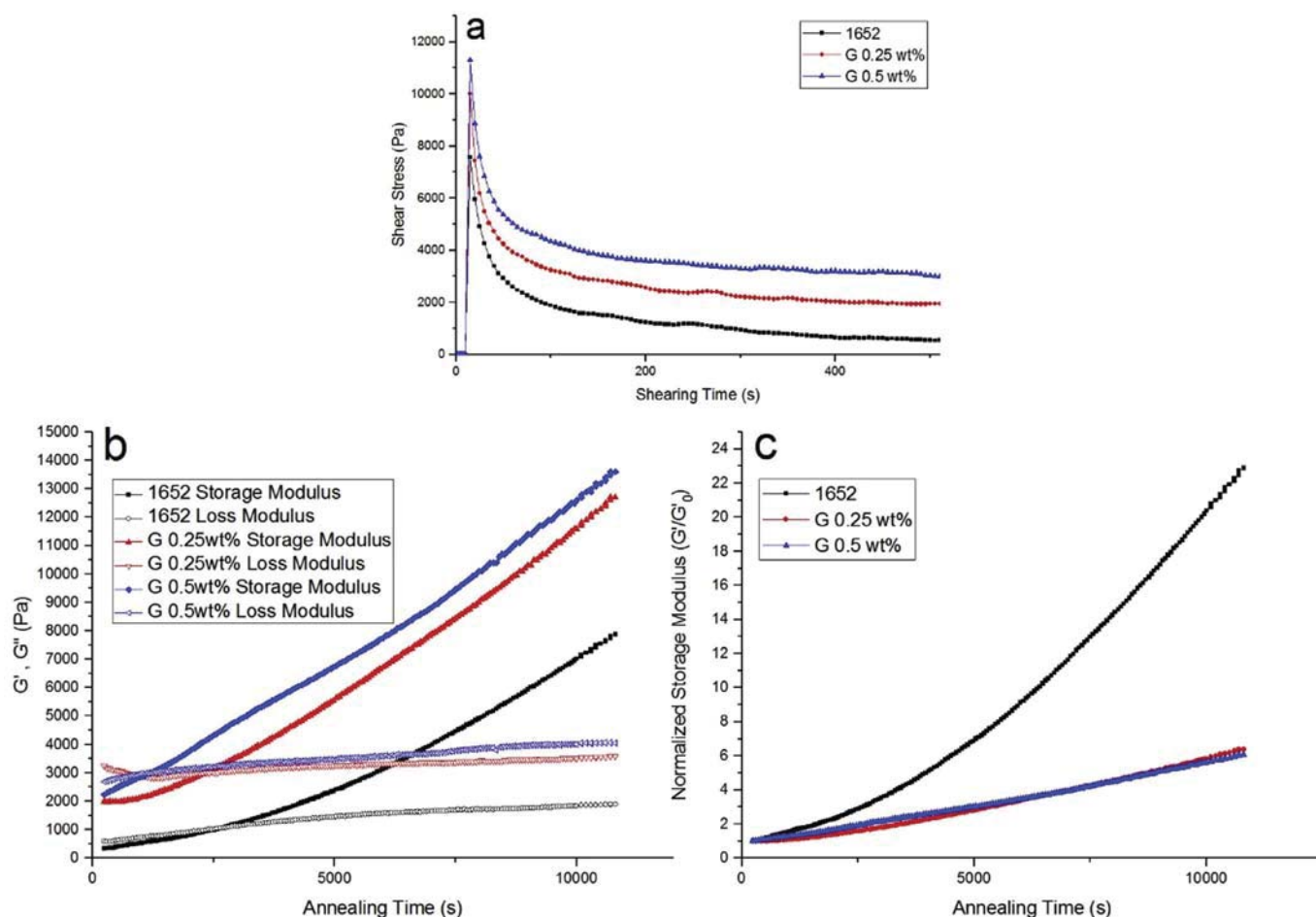
9

Fig. 9. a) Stress as a function of time, b) Storage and Loss modulus recovery and c) normalized storage modulus after cessation of flow with shear rate of 1 s⁻¹ for SEBS 1652 nanocomposite samples containing graphene at T = 220 °C.

behavior could be observed to that of CNT/BCP nanocomposites. However, the results indicate that the presence of graphene nanosheets in BCP leads to higher stress overshoot and steady state stress in startup flow experiment followed by higher value of storage modulus after cessation of flow and slower kinetic of restructuring in comparison to CNT filled samples.

The above results reveal the fact that graphene nanosheets have stronger effect on strengthening the network of BCP nanocomposites than CNT, according to the stronger confinement effect of graphene nanosheets, which results in higher stress overshoot and also incomplete structure breakdown during flow.

Additionally, the reorientation motion of graphene and BCP domains is significantly restrained by the interaction between graphene and neighboring BCP domains and the escape of BCP domains and graphene nanosheets from cages formed by their neighbors via Brownian motion would be remarkably restricted.

3.5. Dynamic mechanical thermal analysis

DMTA is a method of analysis that is widely used to determine the materials' properties as a function of temperature. The ratio of viscous modulus to elastic one ($\tan\delta = E''/E'$) is characterized as damping factor. The temperature associated to the peak in damping factor versus temperature plot is an indication of transition in material due to the molecular motion.

Fig. 10a shows the results of damping factor ($\tan(\delta)$) vs.

temperature for neat BCPs with different PS content (SEBS 1657, SEBS 1652 and SEBS 1537). It can be observed that BCPs exhibit two distinct peaks at around −30 °C and 80−100 °C which are attributed to the glass transition temperature of EB (ethylene-buthylene) domains and PS domains, respectively. These results also show an additional damping peak at around 40−50 °C corresponding to the damping of the interphase region. Interestingly, the interphase damping temperature is almost the same for all three BCP samples, while the damping value increases with increasing the PS content of BCP.

This interphase is a transitional region between adjacent pure PS and EB domains where the chain segments of both blocks coexist. According to Zhou et al. [35], small weak crystalline of EB segments exists within both EB domains and phase interphase. At the interphase region, these EB crystallines are surrounded by PS chain segments. As these weak crystals of EB segments melt at around 25−55 °C, chain segmental movement of the surrounding PS segments occurs within phase interphase which leads to a peak of $\tan(\delta)$ at the above-mentioned temperature.

As is evident, by enhancing the PS content in BCP, the area and the height of $\tan(\delta)$ of the interphase region would be increased, while the corresponding area of PS domains would be decreased. From the above-mentioned results, one could easily realize that in BCP with higher PS content, more PS chain segments are likely to be restricted in interphase region instead of arrangement in PS domains.

From the results of temperature sweep test discussed above, it was explained that increasing the PS content of BCP acts in the favor of thermodynamic incompatibility, which in turn promote the tendency as well as the kinetics of microphase separation. However, this argument is applicable for isothermal condition, while the room temperature cooling used in the present paper (non-isothermal condition, the prepared samples were subjected to room temperature immediately after processing at the temperature of 220 °C) may be too fast for microphase separation of BCP containing high PS content. In this way, a fraction of PS segments may be trapped in the interphase region as the result of incomplete microphase separation. In other words, kinetic parameters dominate the phase separation process.

Fig. 10 also exhibits tan(δ) vs. temperature for BCP nanocomposite samples containing 0.5 wt% MWCNT or graphene nanosheets. It could be observed that the addition of nanofillers results in reducing in the area of tan(δ) of interphase region and PS domains.

The presence of nanofillers could influence BCP microphase separation in different manner based on the thermodynamic (entropic and enthalpic) interactions of nanofillers with BCP segments. There are three possible mechanisms to explain the aforementioned data:

i) Preferential interaction of nanofillers with one of the two segments leads to increasing the segmental incompatibility of BCP. This increased interfacial interaction can also result in decreasing the entropic energy of the system through slowing down the segmental motion. These two effects promote microphase separation. Improved microphase separation drives more PS segments to be arranged in PS domains instead of interphase region. Therefore, PS chain segmental movement would be more restrained. In this case, the area of tan(δ) of both interphase region and PS domains would be decreased due to lower content of PS segments in interphase region and also restriction of segments in PS domains, respectively.

ii) Hindrance effect of incorporated nanofillers could result in disordering of polymer chains and reducing the PS domain formation resulting in higher area of tan(δ).

iii) Nanofillers could also have negligible influence on BCP microphase separation. However, the preferential interactions of nanofillers with BCP segments would render the chain segmental movement and reduce the area of tan(δ) of the corresponding domains.

From the above-mentioned mechanisms and observed DMTA results discussed earlier (decreasing the area of tan(δ) of interphase
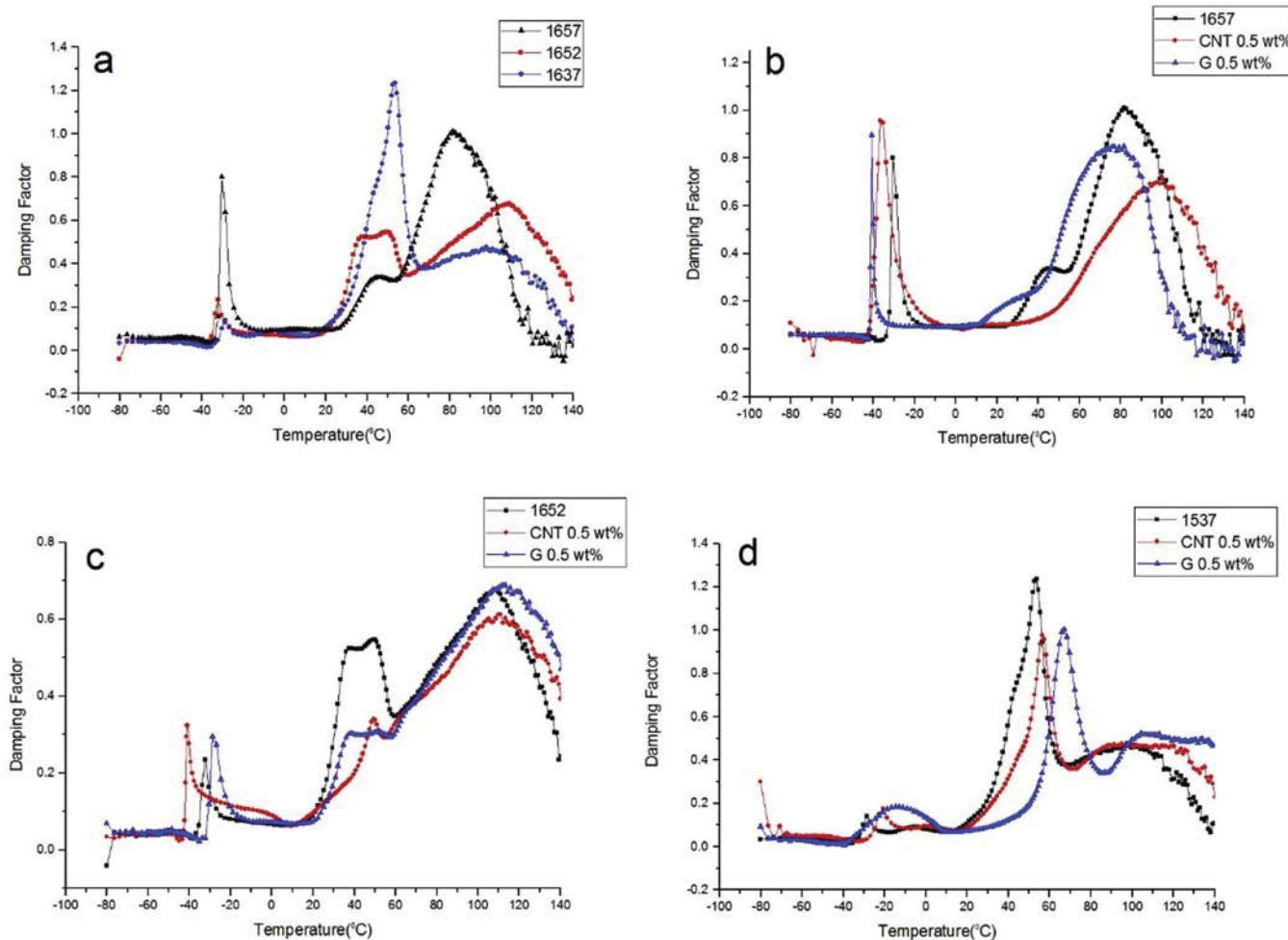

Fig. 10. tan δ versus temperature for a) neat block copolymers (SEBS 1657, SEBS 1652, and SEBS 1537), (b) SEBS 1657, (c) SEBS 1652, and (d) SEBS 1537 block copolymers nanocomposite samples containing 0.5 wt% nanofillers.

region and PS domain), we can conclude that nanofillers could not preclude BCP phase separation (second mechanism).

From the thermodynamic point of view, PS segments are more susceptible to interact with both types of nanofillers (MWCNT and graphene). Enthalpically, the greater affinity of PS segments with nanofillers stems from intermolecular interaction of conjugated π electron of PS segments with electron rich molecules of MWCNT or graphene nanoplates. Entropically, nanofillers cause stretching of polymer chains in the vicinity of nanofillers. Ginzburg considered this entropic contribution as "entropic surface tension" which is insensitive to the nature of chains [36]. Consequently, adsorption of PS segments on the surface of nanofillers would be preferred due to the aromatic, rigid-like nature of PS chains, which undergo less stretching in the vicinity of nanofillers' surface in comparison with the flexible EB rubbery segments which encounter more entropic penalty in backbone.

The preferential interactions of PS segments with nanofillers imply that, if the third mechanism is applicable, SEBS 1537 nanocomposite samples should display a higher reduction in the area of tan(δ) of the interphase region in comparison with the other two BCP nanocomposite samples due to the higher content of PS which could interact with nanofillers (stronger interaction with nanofillers, lower mobility of PS segments).

Following the aforementioned discussion, it could be concluded that nanofillers enhance the ability of BCP to microphase separate and form distinct domains, which is in complete agreement with temperature sweep results.

Furthermore, it could be observed that nanofillers could not dramatically influence the microphase separation of SEBS 1537. It can be seen that incorporation of nanofillers results in a slight decrease in the area of tan(δ) of the interphase region while shifting the peak position to the higher temperature. As it was indicated in temperature sweep experiment (Fig. 7), considerable interaction of PS segments in SEBS 1537 BCP (containing 60 wt% PS) with nanofillers could have two opposing effect on phase separation process. Accordingly, nanoparticle could not induce any noticeable influence on BCP microphase separation. Hence, only a slight decrease in the area of tan(δ) of the interphase region is observed. However, slower dynamic of PS segments in the interphase region caused by strong interactions between PS segments and nanofillers leads to shifting the interphase peak position to higher temperatures. It is worth noting that according to the enhanced confinement effect of graphene nanosheets in comparison with MWCNT, the interphase peak position of graphene filled BCP shifts to higher temperature.

In order to investigate the effect of annealing, BCP samples (SEBS 1652 and SEBS 1537) were annealed in vacuum oven at 130 °C overnight.

The results of tan(δ) vs. temperature obtained for neat BCPs having been annealed are shown in Fig. 11. By a close look at the results, one can easily recognize that annealing influences all three damping peaks, increasing the area of first peak associated to EB domains while decreasing the area of tan(δ) of the interphase region and PS domains with shifting the interphase peak position to higher temperatures.

It is well-documented that thermal annealing could allow the polymer chains to be arranged in their thermodynamically equilibrium morphology.

Here, it could be observed that the annealing results in promoting microphase separation. However, as seen, it is improbable for BCP samples to attain their equilibrium structure by pulling out all the PS segments from interphase region. Therefore, a fraction of PS segments would remain in interphase region. Annealing could also facilitate restructuring of PS segment units within interphase region and PS domains.

Such slightly enhanced microstructural development and also local PS segmental arrangement leads to constraining the PS chain segments. Consequently, the interphase peak position shifts to higher temperature and the area of tan(δ) of the interphase region and PS domains decrease. The increase in the area of first peak could be attributed to the larger number of EB segments in the rubbery EB domain due to the improved microphase separation.

Moreover, by comparing the DMTA result of annealed SEBS 1537 BCP with that obtained for annealed SEBS 1652 BCP, it could be realized that the annealing has no appreciable effect on promoting the microstructure and also restructuring of PS segments. This behavior indicates that the temperature used for annealing SEBS 1537 BCP is not high enough to improve phase separation and reorganization of PS segments. This result is in complete agreement with that discussed in temperature sweep experiment (Fig. 6). As it was observed, SEBS 1537 BCP exhibits microphase separation temperature at 136 °C which is well above the temperature used for annealing in this experiment. Hence, thermodynamic forces are not strong enough to complete microphase separation.

The results of similar experiments performed on BCP nanocomposite samples after being annealed are shown in Fig. 12. The annealing exhibited a similar influence on the behavior of nanocomposite samples as to that of neat BCP matrix. Increasing the area of tan(δ) of EB domain while decreasing the area of tan(δ) of PS domain and shifting the position of interphase region peak to higher temperatures are all associated to the development of microphase separation and local restructuring of PS segments. It should be noted, however, that the area of tan(δ) of interphase region remains unchanged after annealing. These results confirm the previously discussed mechanism (Fig. 7), i.e., that incorporation of nanofillers can enhance the microphase separation of BCP and let the BCP to reach its thermodynamically equilibrium structure. Consequently, annealing would mainly reorganize the arrangement of PS segments in interphase region and PS domains.

4. Conclusions

The present study describes a comprehensive study on the microphase separation behavior of BCP/NP composites. To the best of our knowledge, this is the first attempt to extensively compare BCP morphologies of the same chemical composition (SEBS with spherical, cylindrical and lamella structure), with nanocomposites obtained by adding sheet-like and tube-shaped nanofillers (graphene and CNT). The nanocomposites have been prepared by melt compounding. TEM images of ultracryomicrotome-sliced samples confirm the good dispersion of the nanofillers into the BCP matrices, while SAXS spectra confirm that the microstructure of the BCP is not affected by the presence of the nanofillers.

Melt linear viscoelastic experiments proved to be capable of providing great insight into understanding the involved mechanisms of nanofillers' dispersion in matrix. The results indicate that in nanocomposite samples containing CNT, high thermodynamic affinity between CNT/matrix and also low matrix viscosity is needed to facilitate the diffusion of matrix chains in to CNT aggregates and their dispersion. However, in graphene filled samples, the extent of graphene intercalation is highly dependent on matrix viscosity and therefore the extent of convective forces applied to system during melt mixing.

Temperature sweep measurements indicate that the addition of nanofillers enhances the microphase separation temperature and accelerates its kinetic, mainly due to the confinement of BCP segments. Such confinement restricts the segmental mobility and, hence the enthalpic energy starts to dominate over the entropic one and microphase separated structures are formed. Furthermore, graphene nanosheets show to have more significant effect on microphase separation behavior due to the constructing a more
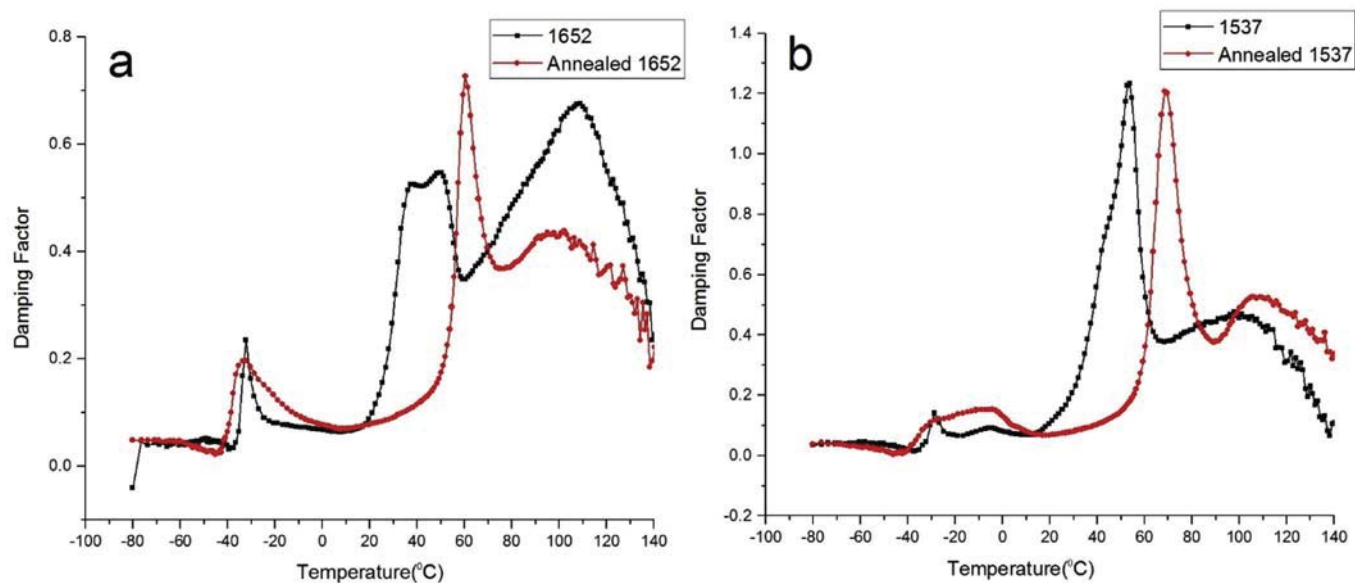
Fig. 11. tan δ versus temperature for (a) SEBS 1652, and (b) SEBS 1537 block copolymers after being annealed.

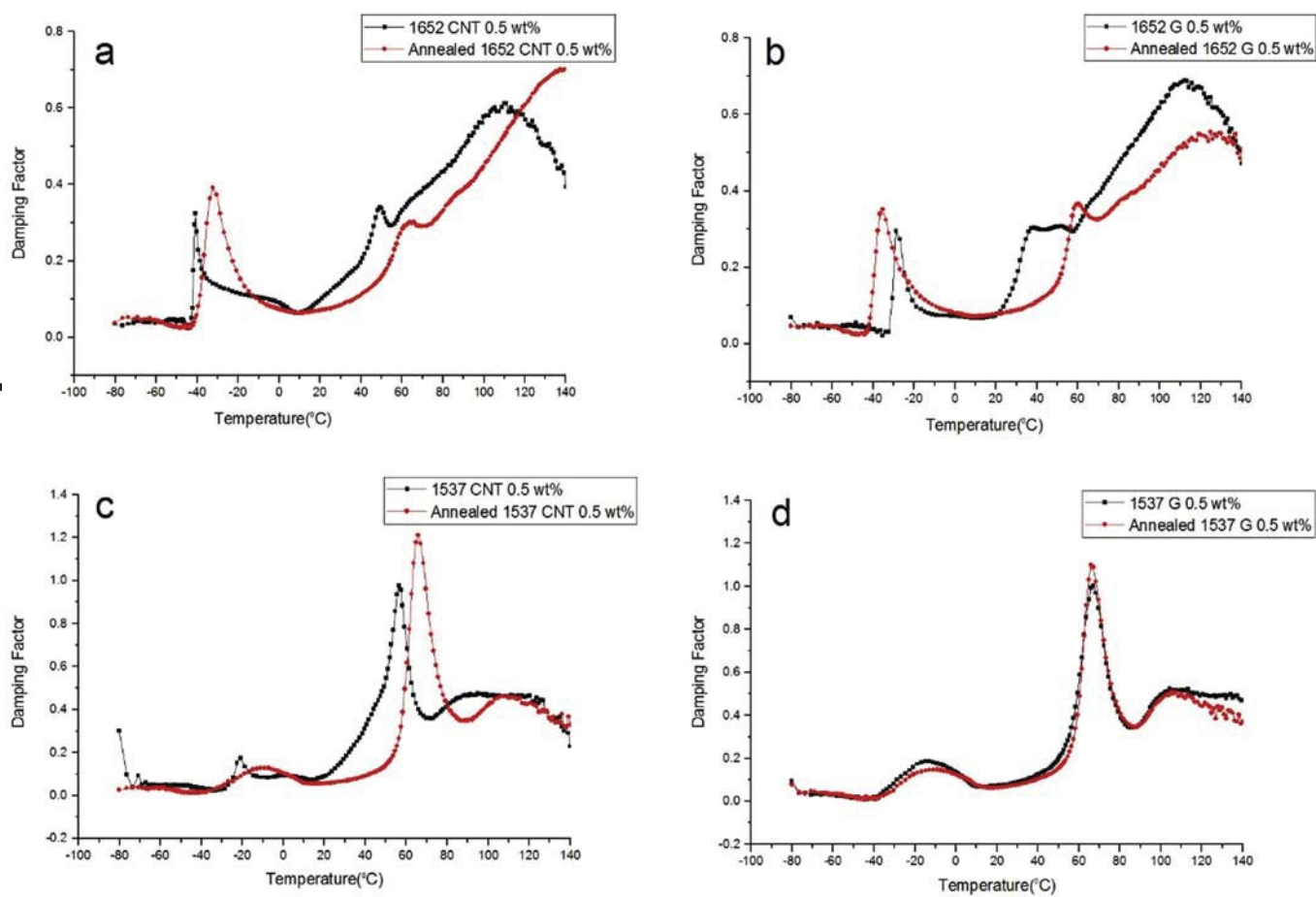**Fig. 12.** tan δ versus temperature for SEBS 1652 nanocomposite samples containing 0.5 wt% a) MWCNT, b) graphene, and SEBS 1537 nanocomposite samples containing 0.5 wt% c) MWCNT, d) graphene, after being annealed.

constrained space in comparison to CNTs.

The orientation and restructuring behavior of BCP nano-composite samples were examined by transient viscoelastic analysis. Higher stress overshoot, incomplete structural breakdown during flow and also slower kinetic of restructuring in nano-composite samples in comparison with neat BCP implies the existence of special 3D network microstructure induced by NPs/domains interactions.

Finally, detailed investigation of DMTA results show that BCP samples exhibit three peaks associated to the damping of EB domains, interphase region and PS domains. The findings show that incorporation of nanofillers reduces the damping of interphase region, mainly due to the enhanced ability of BCP microphase separation. As evidenced by DMTA, thermal annealing results in the development of BCP microphase separation as well as local restructuring of PS segments existing within interphase region and PS domains.

The insights gained from this study clarify the influence of two important parameters on the BCP microphase separation behavior: the relative weight of BCP segments (the morphological structure of BCP), and NPs geometry.

Acknowledgments

References

[1] B.H. Kim, J.Y. Kim, S.O. Kim, S.Y. Park, P.B. Messersmith, I.S. Choi, et al., Directed self-assembly of block copolymers for universal nanopatterning, Soft Matter 9 (2013) 2780, http://dx.doi.org/10.1039/c2sm27535j.

[2] M. Grzelczak, J. Vermant, E.M. Furst, L.M. Liz-Marzán, Directed self-assembly of nanoparticles, ACS Nano 4 (2010) 3591–3605, http://dx.doi.org/10.1021/nn100869j.

[3] G.H. Fredrickson, F.S. Bates, Dynamics of block copolymers: theory and experiment, Annu. Rev. Mater Sci. 26 (1996) 501–550, http://dx.doi.org/10.1146/annurev.ms.26.080196.002441.

[4] J.K. Kim, S.Y. Yang, Y. Lee, Y. Kim, Functional nanomaterials based on block copolymer self-assembly, Prog. Polym. Sci. 35 (2010) 1325–1349, http://dx.doi.org/10.1016/j.progpolymsci.2010.06.002.

[5] F.S. BATES, Polymer-polymer phase behavior, Science 251 (1991) 898–905, http://dx.doi.org/10.1126/science.251.4996.898.

[6] F.S. Bates, G.H. Fredrickson, Block copolymers—designer soft materials, Phys. Today 52 (1999) 32–38, http://dx.doi.org/10.1063/1.882522.

[7] Y. Mai, A. Eisenberg, R.J.M. Nolte, Hest JCM. van, S.P. Armes, A.J. Ryan, et al., Self-assembly of block copolymers, Chem. Soc. Rev. 41 (2012) 5969, http://dx.doi.org/10.1039/c2cs35115c.

[8] S.B. Darling, Directing the self-assembly of block copolymers, Prog. Polym. Sci. 32 (2007) 1152–1204, http://dx.doi.org/10.1016/j.progpolymsci.2007.05.004.

[9] Y.H. Ha, Y. Kwon, T. Breiner, E.P. Chan, T. Tzianetopoulou, R.E. Cohen, et al., An orientationally ordered hierarchical exfoliated clay-block copolymer nano-composite, Macromolecules 38 (2005) 5170–5179, http://dx.doi.org/10.1021/ma0476792.

[10] R. Krishnamoorti, A.S. Silva, C.A. Mitchell, Effect of silicate layer anisotropy on cylindrical and spherical microdomain ordering in block copolymer nano-composites, J. Chem. Phys. 115 (2001) 7175–7181, http://dx.doi.org/10.1063/1.1403004.

[11] D.J. Carastan, N.R. Demarquette, A. Vermogen, K. Masenelli-Varlot, Linear viscoelasticity of styrenic block copolymers—clay nanocomposites, Rheol. Acta 47 (2008) 521–536, http://dx.doi.org/10.1007/s00397-008-0283-2.

[12] S. Choi, K.M. Lee, C.D. Han, Effects of triblock copolymer architecture and the degree of functionalization on the organoclay dispersion and rheology of nanocomposites, Macromolecules 37 (2004) 7649–7662, http://dx.doi.org/10.1021/ma030585s.

[13] D.J. Carastan, L.G. Amurin, A.F. Craievich, M.D.C. Gonalves, N.R. Demarquette, Clay-containing block copolymer nanocomposites with aligned morphology prepared by extrusion, Polym. Int. 63 (2014) 184–194, http://dx.doi.org/10.1002/pi.4480.

[14] A. Vazquez, M. López, E. Serrano, A. Valea, N.E. Zafeiropoulos, I. Mondragon, Structural and ordering behavior of lamellar polystyrene- *block* -poly-butadiene- *block* -polystyrene triblock copolymer containing layered silicates, J. Appl. Polym. Sci. 110 (2008) 3624–3637, http://dx.doi.org/10.1002/app.28885.

[15] S. Iijima, Helical microtubules of graphitic carbon, Nature 354 (1991) 56–58, http://dx.doi.org/10.1038/354056a0.

[16] H. Garate, M.L. Fascio, I. Mondragon, N.B. D'Accorso, S. Goyanes, Surfactant-aided dispersion of polystyrene-functionalized carbon nanotubes in a nano-structured poly(styrene-b-isoprene-b-styrene) block copolymer, Polym. Guildf. 52 (2011) 2214–2220, http://dx.doi.org/10.1016/j.polymer.2011.03.032.

[17] T. Hosseini-Sianaki, H. Nazockdast, B. Salehnia, E. Nazockdast, Microphase separation and hard domain assembly in thermoplastic polyurethane/multi-walled carbon nanotube nanocomposites, Polym. Eng. Sci. 55 (2015) 2163–2173, http://dx.doi.org/10.1002/pen.24101.

[18] G. Mittal, V. Dhand, K.Y. Rhee, S.-J. Park, W.R. Lee, A review on carbon nanotubes and graphene as fillers in reinforced polymer nanocomposites, J. Ind. Eng. Chem. 21 (2015) 11–25, http://dx.doi.org/10.1016/j.jiec.2014.03.022.

[19] I. Szleifer, R. Yerushalmi-Rozen, Polymers and carbon nano-tubes—dimensionality, interactions and nanotechnology, Polym. Guildf. 46 (2005) 7803–7818, http://dx.doi.org/10.1016/j.polymer.2005.05.104.

[20] S.K. Yadav, S.S. Mahapatra, J.W. Cho, J.Y. Lee, Functionalization of multiwalled carbon nanotubes with poly(styrene- *b* -(ethylene- *co* -butylene)- *b* -styrene) by click coupling, J. Phys. Chem. C 114 (2010) 11395–11400, http://dx.doi.org/10.1021/jp1028382.

[21] L. Peponi, A. Tercjak, J. Gutierrez, M. Cardinali, I. Mondragon, L. Valentini, et al., Mapping of carbon nanotubes in the polystyrene domains of a polystyrene-b-polyisoprene-b-polystyrene block copolymer matrix using electrostatic force microscopy, Carbon N. Y. 48 (2010) 2590–2595, http://dx.doi.org/10.1016/j.carbon.2010.03.062.

[22] L. Peponi, L. Valentini, L. Torre, I. Mondragon, J.M. Kenny, Surfactant assisted selective confinement of carbon nanotubes functionalized with octadecyl-amine in a poly(styrene-b-isoprene-b-styrene) block copolymer matrix, Carbon N. Y. 47 (2009) 2474–2480, http://dx.doi.org/10.1016/j.carbon.2009.04.039.

[23] M. Ilčíková, M. Mrlík, T. Sedláček, D. Chorvát, I. Krupa, M. Šlouf, et al., Visco-elastic and photo-actuation studies of composites based on polystyrene-grafted carbon nanotubes and styrene-b-isoprene-b-styrene block copol-ymer, Polym. Guildf. 55 (2014) 211–218, http://dx.doi.org/10.1016/j.polymer.2013.11.031.

[24] J.R. Potts, D.R. Dreyer, C.W. Bielawski, R.S. Ruoff, Graphene-based polymer nanocomposites, Polym. Guildf. 52 (2011) 5–25, http://dx.doi.org/10.1016/j.polymer.2010.11.042.

[25] A. Rostami, H. Nazockdast, M. Karimi, D. Acierno, G. Filippone, K.C. Kemp, et al., Graphene induced microstructural changes of PLA/MWCNT biodegradable nanocomposites: rheological, morphological, thermal and electrical proper-ties, RSC Adv. 6 (2016) 49747–49759, http://dx.doi.org/10.1039/C6RA08345E.

[26] C. Mao, J. Huang, Y. Zhu, W. Jiang, Q. Tang, X. Ma, Tailored parallel graphene stripes in plastic film with conductive anisotropy by shear-induced self-as-sembly, J. Phys. Chem. Lett. 4 (2013) 43–47, http://dx.doi.org/10.1021/jz301811b.

[27] H. Nazockdast, Morphology and Structure of Polymer Blends Containing Nanofillers, Encycl. Polym. Blends, Wiley-VCH Verlag GmbH & Co. KGaA, Weinheim, Germany, 2016, pp. 401–482, http://dx.doi.org/10.1002/9783527653966.ch7.

[28] C.D. Han, Polymer Rheology, Oxford University Press, 2007.

[29] G.P. Kar, A. Bharati, P. Xavier, G. Madras, S. Bose, B.A. Wolf, et al., The key role of polymer grafted nanoparticles in the phase miscibility of an LCST mixture, Phys. Chem. Chem. Phys. 17 (2015) 868–877, http://dx.doi.org/10.1039/C4CP02925A.

[30] S. Xin, Y. Li, H. Zhao, Y. Bian, W. Li, C. Han, et al., Confinement crystallization of poly(l-lactide) induced by multiwalled carbon nanotubes and graphene nanosheets, J. Therm. Anal. Calorim. 122 (2015) 379–391, http://dx.doi.org/10.1007/s10973-015-4695-9.

[31] S. Aoyama, Y.T. Park, T. Ougizawa, C.W. Macosko, Melt crystallization of poly(ethylene terephthalate): comparing addition of graphene vs. carbon nanotubes, Polym. Guildf. 55 (2014) 2077–2085, http://dx.doi.org/10.1016/j.polymer.2014.02.055.

[32] B. Ranjbar, H. Nazockdast, Shear flow-induced orientation and structural re-covery of multiwalled carbon nanotube in poly(ethylene oxide) matrix, J. Appl. Polym. Sci. 132 (2015), http://dx.doi.org/10.1002/app.41753 n/a-n/a.

[33] F. Khalkhal, P.J. Carreau, Critical shear rates and structure build-up at rest in MWCNT suspensions, J. Nonnewt. Fluid Mech. 171 (2012) 56–66, http://dx.doi.org/10.1016/j.jnnfm.2012.01.008.

[34] H. Kim, C.W. Macosko, Processing-property relationships of polycarbonate/graphene composites, Polym. Guildf. 50 (2009) 3797–3809, http://dx.doi.org/10.1016/j.polymer.2009.05.038.

[35] T. Zhou, A. Zhang, C. Zhao, H. Liang, Z. Wu, J. Xia, Molecular chain movements and transitions of SEBS above room temperature studied by moving-window

two-dimensional correlation infrared spectroscopy, Macromolecules 40 (2007) 9009–9017, http://dx.doi.org/10.1021/ma071630p.

[36] V.V. Ginzburg, Influence of nanoparticles on miscibility of polymer blends. a simple theory, Macromolecules 38 (2005) 2362–2367, http://dx.doi.org/10.1021/ma0482821.

[37] I.W. Hamley, V. Castelletto, Small-angle scattering of block copolymers: in the melt, solution and crystal states, Prog. Polym. Sci. 29 (2004) 909–948, http://dx.doi.org/10.1016/j.progpolymsci.2004.06.001.

[38] J.K. Kim, H.H. Lee, S. Sakurai, S. Aida, J. Masamoto, S. Nomura, et al., Lattice disordering and domain dissolution transitions in polystyrene- block -poly(-ethylene- co -but-1-ene)- block -polystyrene triblock copolymer having a highly asymmetric composition, Macromolecules 32 (1999) 6707–6717, http://dx.doi.org/10.1021/ma9902854.